

# The computation aspects of the equivalent-layer technique: review and perspective

Diego Takahashi<sup>1,\*</sup>, André L. A. Reis<sup>2</sup>, Vanderlei C. Oliveira Jr.<sup>1</sup> and Valéria C. F. Barbosa<sup>1</sup>

<sup>1</sup>*Observatório Nacional, Department of Geophysics, Rio de Janeiro, Brasil*

<sup>2</sup>*Universidade do Estado do Rio de Janeiro, Department of Applied Geology, Rio de Janeiro, Brasil*

Correspondence\*: Valéria C.F. Barbosa  
valcris@on.br

## 2 ABSTRACT

3 Equivalent-layer technique is a powerful tool for processing potential-field data in the space  
4 domain. However, the greatest hindrance for using the equivalent-layer technique is its high  
5 computational cost for processing massive data sets. The large amount of computer memory  
6 usage to store the full sensitivity matrix combined with the computational time required for matrix-  
7 vector multiplications and to solve the resulting linear system, are the main drawbacks that made  
8 unfeasible the use of the equivalent-layer technique for a long time. More recently, the advances in  
9 computational power propelled the development of methods to overcome the heavy computational  
10 cost associated with the equivalent-layer technique. We present a comprehensive review of the  
11 computation aspects concerning the equivalent-layer technique addressing how previous works  
12 have been dealt with the computational cost of this technique. Historically, the high computational  
13 cost of the equivalent-layer technique has been overcome by using a variety of strategies such as:  
14 moving data-window scheme, equivalent data concept, wavelet compression, lower-dimensional  
15 subspace, quadtree discretization, reparametrization of the equivalent layer by a piecewise-  
16 polynomial function, iterative scheme without solving a system of linear equations and the  
17 convolutional equivalent layer using the concept of block-Toeplitz Toeplitz-block (BTTB) matrices.  
18 We compute the number of floating-point operations of some of these strategies adopted in the  
19 equivalent layer technique to show their effectiveness in reducing the computational demand.  
20 Numerically, we also address the stability of some of these strategies used in the equivalent  
21 layer technique by comparing with the stability via the classic equivalent-layer technique with the  
22 zeroth-order Tikhonov regularization.

23 **Keywords:** equivalent layer, gravimetry, fast algorithms, computational cost, stability analysis

## 1 INTRODUCTION

In accord with potential theory, a continuous potential-field data (gravity and magnetic data) produced by any source can be exactly reproduced by a continuous and infinite 2D physical-property surface distribution that is called the equivalent layer. The equivalent layer is a mathematical solution of Laplace's equation in the source-free region with the observed potential-field data as the Dirichlet boundary condition (Kellogg, 1929). Grounded on well-established potential theory, the equivalent-layer technique has been used by exploration geophysicists for processing potential-field data since the late 1960s (Dampney, 1969).

Although there was always a great demand for gravity and magnetic data processing, the equivalent-layer technique has not been massively used. This occurs because its high computational cost makes the equivalent-layer technique computationally inefficient for processing massive data sets. In the classic equivalent-layer technique, the continuous problem of the equivalent layer involving integrals is approximated by a discrete form of the equivalent layer. First, a discrete and finite set of equivalent sources (point masses, prisms, magnetic dipoles, doublets) is arranged in a layer with finite horizontal dimensions and located below the observation surface. Next, a linear system of equations is set up with a large and full sensitivity matrix. Then, a regularized linear inverse problem is solved to estimate the physical property of each equivalent source within the discrete equivalent layer subject to fitting a discrete set of potential-field observations. Finally, the estimated physical-property distribution within the equivalent layer is used to accomplish the desired processing of the potential-field data (e.g., interpolation, upward/downward continuation, reduction to the pole). The latter step is done by multiplying the matrix of Green's functions associated with the desired transformation by the estimated physical-property distribution.

Beginning in the late 1980s, the equivalent-layer techniques computationally efficient have arose. To our knowledge, the first method towards improving the efficiency was proposed by Leão and Silva (1989) who used an overlapping moving-window scheme spanning the data set. The strategy adopted in Leão and Silva (1989) involves solving several smaller, regularized linear inverse problems instead of one large problem. This strategy uses a small data window and distributes equivalent sources on a small regular grid at a constant depth located below the data surface. Leão and Silva (1989) ensure that sources window extends beyond the boundaries of the data window. For each position of the data window, this scheme consists in computing the processed field at the center of the data window only and the next estimates of the processed field are obtained by shifting the data window across the entire dataset. Recently, Soler and Uieda (2021) developed a computational approach to increase the efficiency of the equivalent-layer technique by combining two strategies. The first one — the block-averaging source locations — reduces the model parameters and the second strategy — the gradient-boosted algorithm — reduces the size of the linear system to be solved by fitting the equivalent source model iteratively along overlapping windows. Notice that the equivalent-layer strategy of using a moving-window scheme either in Leão and Silva (1989) or in Soler and Uieda (2021) is similar to discrete convolution.

In another approach to reduce computational workload of the equivalent-layer technique Mendonça and Silva (1994) developed an iterative procedure by incorporating one data point at a time and thus selecting a smaller data set. This strategy adopted by Mendonça and Silva (1994) is known as 'equivalent data concept'. Li and Oldenburg (2010) transformed the full sensitivity matrix into a sparse one using the compression of the coefficient matrix via wavelet transforms based on the orthonormal compactly supported wavelets. For jointly processing the components of gravity-gradient data using the equivalent-source processing, Barnes and Lumley (2011) applied the quadtree model discretization to generate a sparse linear system of equations. Davis and Li (2011) adaptively discretized the model (quadtree model discretization) based on localized anomalies and used wavelet transforms to reduce, reordered the model parameters (Hilbert

67 space-filling curves) and compressed each row of the sensitivity matrix of the reordered parameter set  
68 (wavelet transforms). By using the subspace method, Mendonça (2020) reduced the dimension of the  
69 linear system of equations to be solved in the equivalent-layer technique. The subspace bases span the  
70 parameter-model space and they are constructed by applying the singular value decomposition to the matrix  
71 containing the gridded data. These strategies followed by Li and Oldenburg (2010), Barnes and Lumley  
72 (2011), Davis and Li (2011) and Mendonça (2020) may be grouped into the strategy of compression  
73 approaches to solve large linear system of equations.

74 Following the strategy of reparametrization of the equivalent layer, Oliveira Jr. et al. (2013) reduced the  
75 model parameters by approximating the equivalent-source layer by a piecewise-polynomial function defined  
76 on a set of user-defined small equivalent-source windows. The estimated parameters are the polynomial  
77 coefficients for each window and they are much smaller than the original number of equivalent sources.  
78 Siqueira et al. (2017) developed an iterative solution where the sensitivity matrix is transformed into a  
79 diagonal matrix with constant terms through the use of the 'excess mass criterion' and of the positive  
80 correlation between the observed gravity data and the masses on the equivalent layer. Jirigalatu and Ebbing  
81 (2019) combined the Gauss-fast Fourier transform (FFT) with Landweber's algorithm and proposed a  
82 fast equivalent-layer technique for jointly processing two-components of the gravity-gradient data. The  
83 Landweber's algorithm has some similarities with gradient-descent algorithm. The strategies worked  
84 out by Siqueira et al. (2017) and Jirigalatu and Ebbing (2019) avoid calculating the Hessian matrix and  
85 solving linear system of equations.

86 Recently, Takahashi et al. (2020, 2022), developed fast and effective equivalent-layer techniques for  
87 processing, respectively, gravity and magnetic data by modifying the forward modeling to estimate the  
88 physical-property distribution over the layer through a 2D discrete convolution that can be efficiently  
89 computed via 2D FFT. These methods took advantage of the Block-Toeplitz Toeplitz-block (BTTB)  
90 structure of the sensitivity matrices, allowing them to be calculated by using only their first column. In  
91 practice, the forward modeling uses a single equivalent source, which significantly reduces the required  
92 RAM memory. Takahashi et al. (2020, 2022) employed the strategy of the convolutional equivalent layer  
93 using the concept of BTTB matrices.

94 Here, we present a comprehensive review of

## 2 THE EQUIVALENT-LAYER TECHNIQUE

### 95 2.1 Fundamentals

96 Consider a set of  $N$  potential-field observations (gravity or magnetic data)  $d_i^o(x_i, y_i, z_i)$ ,  $i = 1, \dots, N$ ,  
 97 at the  $i$ th observation point  $(x_i, y_i, z_i)$  of a Cartesian coordinate system with  $x$ -,  $y$ - and  $z$ -axis pointing to  
 98 north, east and down, respectively. Physically, the discrete set of potential-field observations is produced by  
 99 a unknown source distribution in the subsurface. Mathematically, it represents a discrete set of a harmonic  
 100 function.

101 A standard way to deal with the classical equivalent-layer technique is approximate the observed potential-  
 102 field data by the predicted data, which in turn are produced by a fictitious layer of sources, called equivalent  
 103 layer. The equivalent layer is located below the observation surface, at depth  $z_0$  ( $z_0 > z_i$ ), and with finite  
 104 horizontal dimensions being composed by a finite discrete set of equivalent sources (e.g., point masses,  
 105 dipoles, or prisms). Mathematically, this approximation can be written in matrix notation as

$$\mathbf{d} = \mathbf{A}\mathbf{p}, \quad (1)$$

106 where  $\mathbf{d}$  is an  $N$ -dimensional predicted data vector whose  $i$ th element,  $d_i(x_i, y_i, z_i)$ ,  $i = 1, \dots, N$ , is the  
 107 predicted potential-field observation,  $\mathbf{p}$  is an  $M$ -dimensional parameter vector whose  $j$ th element  $p_j$  is a  
 108 physical property of the  $j$ th equivalent source and  $\mathbf{A}$  is the  $N \times M$  sensitivity matrix whose  $ij$ th element  
 109  $a_{ij}$  is a harmonic function.

### 110 2.2 Computational strategies

111 The classical equivalent-layer technique consists of estimating the parameter vector  $\mathbf{p}$  from the  $N$ -  
 112 dimensional observed data vector  $\mathbf{d}^o$  whose  $i$ th element is defined as the  $d_i^o(x_i, y_i, z_i)$ ,  $i = 1, \dots, N$ .  
 113 Usually, this estimate can be obtained by a regularized least-squares solution. The estimated parameter  
 114 is stable, fits the observed data and can be used to yield a desired linear transformation of the data, such  
 115 as interpolation, upward (or downward) continuation, reduction to the pole, joint processing of gravity  
 116 gradient data and more. Mathematically, the desired linear transformation of the data can be obtained by

$$\hat{\mathbf{t}} = \mathbf{T}\mathbf{p}^*, \quad (2)$$

117 where  $\hat{\mathbf{t}}$  is an  $N$ -dimensional transformed data vector,  $\mathbf{p}^*$  is an  $M$ -dimensional estimated parameter vector  
 118 and  $\mathbf{T}$  is the  $N \times M$  matrix of Green's functions whose  $ij$ th element is the transformed field at the  $i$ th  
 119 observation point produced by the  $j$ th equivalent source.

120 The biggest hurdle to use the classical equivalent-layer technique is the computational complexity  
 121 to handle large datasets because the sensitivity matrix  $\mathbf{A}$  (equation 1) is dense. Usually, the estimated  
 122 parameter vector  $\mathbf{p}^*$  requires to solve a large-scale linear inversion which in turn means to deal with  
 123 some obstacles concerning large computational cost: i) the large computer memory to store large and full  
 124 matrices; ii) the long computation time to multiply a matrix by a vector; and iii) the long computation time  
 125 to solve a large linear system of equations.

126 Here, we review some strategies for reducing the computational cost of equivalent-layer technique. These  
 127 strategies are the following:

## 128 2.2.1 The moving data-window scheme

129 Leão and Silva (1989) reduced the total processing time and memory usage of equivalent-layer technique  
 130 by means of a moving data-window scheme. A small moving data window with  $N_w$  observations and  
 131 a small equivalent layer with  $M_w$  equivalent sources ( $M_w > N_w$ ) located below the observations are  
 132 established. For each position of a moving-data window, Leão and Silva (1989) estimate a stable solution  
 133  $\mathbf{p}^*$  by using a data-space approach with the zeroth-order Tikhonov regularization (Aster et al., 2018), i.e.,

$$\mathbf{p}^* = \mathbf{A}^\top \left( \mathbf{A}\mathbf{A}^\top + \mu\mathbf{I} \right)^{-1} \mathbf{d}^o, \quad (3)$$

134 where  $\mu$  is a regularizing parameter,  $\mathbf{I}$  is an identity matrix of order  $N_w$  and the superscript  $\top$  stands for a  
 135 transpose. After estimating an  $M_w \times 1$  parameter vector  $\mathbf{p}^*$  (equation 3) the desired transformation of the  
 136 data is only calculated at the central point of each moving-data window, i.e.:

$$\hat{\mathbf{t}}_k = \mathbf{t}_k^\top \mathbf{p}^*, \quad (4)$$

137 where  $\hat{\mathbf{t}}_k$  is the transformed data calculated at the central point  $k$  of the data window and  $\mathbf{t}_k$  is an  $M_1$  vector  
 138 whose elements form the  $k$ th row of the matrix of Green's functions  $\mathbf{T}$  (equation 2) of the desired linear  
 139 transformation of the data.

140 By shifting the moving-data window with a shift size of one data spacing, a new position of a data  
 141 window is set up. Next, the aforementioned process (equations 3 and 4) is repeated for each position of a  
 142 moving-data window, until the entire data have been processed. Hence, instead of solving a large inverse  
 143 problem, Leão and Silva (1989) solve several much smaller ones.

144 To reduce the size of the linear system to be solved, Soler and Uieda (2021) adopted the same strategy  
 145 proposed, originally, by Leão and Silva (1989) of using a small moving-data window sweeping the whole  
 146 data. In Leão and Silva (1989), a moving-data window slides to the next adjacent data window following a  
 147 sequential movement, the predicted data is calculated inside the data window and the desired transformation  
 148 are only calculated at the center of the moving-data window. Unlike Leão and Silva (1989), Soler and  
 149 Uieda (2021) do not adopt a sequential order of the data windows; rather, they adopt a randomized  
 150 order of windows in the iterations of the gradient-boosting algorithm (Friedman, 2001 and 2002). The  
 151 gradient-boosting algorithm in Soler and Uieda (2021) estimates a stable solution using the data and the  
 152 equivalent sources that fall within a moving-data window; however, it calculates the predicted data and the  
 153 residual data in the whole survey data. Next, the residual data that fall within a new position of the data  
 154 window is used as input data to estimate a new stable solution within the data window which in turn is  
 155 used to calculate a new predicted data and a new residual data in the whole survey data. Finally, unlike  
 156 Leão and Silva (1989), in Soler and Uieda (2021) neither the data nor the equivalent sources need to be  
 157 distributed in regular grids. Indeed, Leão and Silva (1989) built their method using regular grids, but in fact  
 158 regular grids are not necessary. Regarding the equivalent-source layout, Soler and Uieda (2021) proposed  
 159 the block-averaged sources locations in which the survey area is divided into horizontal blocks and one  
 160 single equivalent source is assigned to each block. Each single source per block is placed over the layer  
 161 with its horizontal coordinates given by the average horizontal positions of observation points. According  
 162 to Soler and Uieda (2021), the block-averaged sources layout reduces the number of equivalent sources  
 163 significantly and the gradient-boosting algorithm provides even greater efficiency in terms of data fitting.

## 164 2.2.2 The equivalent-data concept

165 To reduced the total processing time and memory usage of equivalent-layer technique, Mendonça and  
 166 Silva (1994) proposed a strategy called 'equivalent data concept'. The equivalent data concept is grounded  
 167 on the principle that there is a subset of redundant data that does not contribute to the final solution and  
 168 thus can be dispensed. Conversely, there is a subset of observations, called equivalent data, that contributes  
 169 effectively to the final solution and fits the remaining observations (redundant data). Iteratively, Mendonça  
 170 and Silva (1994) selected the subset of equivalent data that is substantially smaller than the original dataset.  
 171 This selection is carried out by incorporating one data point at a time.

172 According to Mendonça and Silva (1994), the number of equivalent data is about one-tenth of the total  
 173 number of observations. These authors used the equivalent data concept to carry out an interpolation of  
 174 gravity data. They showed a reduction of the total processing time and memory usage by, at least, two  
 175 orders of magnitude as opposed to using all observations in the interpolation process via the classical  
 176 equivalent-layer technique.

## 177 2.2.3 The wavelet compression and lower-dimensional subspace

178 For large data sets, the sensitivity matrix  $\mathbf{A}$  (equation 1) is a drawback in applying the equivalent-layer  
 179 technique because it is a large and dense matrix.

180 Li and Oldenburg (2010) transformed a large and full sensitivity matrix into a sparse one by using fast  
 181 wavelet transforms. In the wavelet domain, Li and Oldenburg (2010) applyied a 2D wavelet transform to  
 182 each row and column of the original sensitivity matrix  $\mathbf{A}$  to expand it in the wavelet bases. This operation  
 183 can be done by premultiplying the original sensitivity matrix  $\mathbf{A}$  by a matrix representing the 2D wavelet  
 184 transform  $\mathbf{W}_2$  and then the resulting is postmultiplied by the transpose of  $\mathbf{W}_2$  (i.e.,  $\mathbf{W}_2^\top$ ).

$$\tilde{\mathbf{A}} = \mathbf{W}_2 \mathbf{A} \mathbf{W}_2^\top, \quad (5)$$

185 where  $\tilde{\mathbf{A}}$  is the expanded original sensitivity matrix in the wavelet bases with many elements zero or close  
 186 to zero. Next, the matrix  $\tilde{\mathbf{A}}$  is replaced by its sparse version  $\tilde{\mathbf{A}}_s$  in the wavelet domain which in turn is  
 187 obtained by retaining only the large elements of the  $\tilde{\mathbf{A}}$ . Thus, the elements of  $\tilde{\mathbf{A}}$  whose amplitudes fall  
 188 below a relative threshold are discarded. In Li and Oldenburg (2010), the original sensitivity matrix  $\mathbf{A}$  is  
 189 high compressed resulting in a sparce matrix  $\tilde{\mathbf{A}}_s$  with a few percent of nonzero elements and the regularized  
 190 inverse problem is solved in the wavelet domain by using  $\tilde{\mathbf{A}}_s$ . Finally, the equivalent source, in the space  
 191 domain, is obtained by applying an inverse wavelet transform. For regularly spaced grid of data, Li and  
 192 Oldenburg (2010) reported that high compression ratios are achived with insignificant loss of accuracy.

193 Li and Oldenburg (2010) used the equivalent-layer technique with a wavelet compression to perform an  
 194 upward continuation of total-field anomaly between uneven surfaces. As compared to the upward-continued  
 195 total-field anomaly by equivalent layer using the dense matrix, Li and Oldenburg's (2010) approach, using  
 196 the Daubechies wavelet, decreased CPU (central processing unit) time by up to two orders of magnitude.

197 Mendonça (2020) overcame the solution of intractable large-scale equivalent-layer problem by using the  
 198 subspace method (e.g., Skilling and Bryan, 1984; Kennett et al., 1988; Oldenburg et al., 1993; Barbosa  
 199 et al., 1997). The subspace method reduces the dimension of the linear system of equations to be solved.  
 200 Given a higher-dimensional space (e.g.,  $M$ -dimensional model space,  $\mathbb{R}^M$ ), there exists many lower-  
 201 dimensional subspaces (e.g.,  $Q$ -dimensional subspace) of  $\mathbb{R}^M$ . The linear inverse problem related to the  
 202 equivalent-layer technique consists in finding an  $M$ -dimension parameter vector  $\mathbf{p} \in \mathbb{R}^M$  which adequately  
 203 fits the potential-field data. The subspace method looks for a parameter vector who lies in a  $Q$ -dimensional

204 subspace of  $\mathbb{R}^M$  which, in turn, is spanned by a set of  $Q$  vectors  $\mathbf{v}_i = 1, \dots, Q$ , where  $\mathbf{v}_i \in \mathbb{R}^M$ . In matrix  
205 notation, the parameter vector in the subspace method can be written as

$$\mathbf{p} = \mathbf{V} \boldsymbol{\alpha}, \quad (6)$$

206 where  $\mathbf{V}$  is an  $M \times Q$  matrix whose columns  $\mathbf{v}_i = 1, \dots, Q$  form a basis vectors for a subspace  $Q$  of  $\mathbb{R}^M$ .  
207 In equation 6, the parameter vector  $\mathbf{p}$  is defined as a linear combination in the space spanned by  $Q$  basis  
208 vectors  $\mathbf{v}_i = 1, \dots, Q$  and  $\boldsymbol{\alpha}$  is a  $Q$ -dimensional unknown vector to be determined. The main advantage of  
209 the subspace method is that the linear system of  $M$  equations in  $M$  unknowns to be originally solved is  
210 reduced to a new linear system of  $Q$  equations in  $Q$  unknowns which requires much less computational  
211 effort since  $Q \ll M$ . The choice of the  $Q$  basis vectors  $\mathbf{v}_i = 1, \dots, Q$  (equation 6) in the subspace method  
212 is not strict. Mendonça (2020), for example, chose the eigenvectors yielded by applying the singular value  
213 decomposition of the matrix containing the gridded data set. The number of eigenvectors used to form  
214 basis vectors will depend on the singular values.

215 The proposed subspace method for solving large-scale equivalent-layer problem by Mendonça (2020)  
216 was applied to estimate the mass excess or deficiency caused by causative gravity sources.

## 217 2.2.4 The quadtree discretization

218 To make the equivalent-layer technique tractable, Barnes and Lumley (2011) also transformed the dense  
219 sensitivity matrix  $\mathbf{A}$  (equation 1) into a sparse matrix. In Barnes and Lumley (2011), a sparse version of  
220 the sensitivity matrix is achieved by grouping equivalent sources (e.g., they used prisms) distant from an  
221 observation point together to form a larger prism or larger block. Each larger block has averaged physical  
222 properties and averaged top- and bottom-surfaces of the grouped smaller prisms (equivalent sources) that  
223 are encompassed by the larger block. The authors called it the 'larger averaged block' and the essence of  
224 their method is the reduction in the number of equivalent sources, which means a reduction in the number  
225 of parameters to be estimated implying in model dimension reduction.

226 The key of the Barnes and Lumley's (2011) method is the algorithm for deciding how to group the smaller  
227 prisms. In practice, these authors used a recursive bisection process that results in a quadtree discretization  
228 of the equivalent-layer model.

229 By using the quadtree discretization, Barnes and Lumley (2011) were able to jointly process multiple  
230 components of airborne gravity-gradient data using a single layer of equivalent sources. To our knowledge,  
231 Barnes and Lumley (2011) are the pioneers on processing full-tensor gravity-gradient data jointly. In  
232 addition to computational feasibility, Barnes and Lumley's (2011) method reduces low-frequency noise  
233 and can also remove the drift in time-domain from the survey data. Those authors stressed that the  
234  $G_{zz}$ -component calculated through the single estimated equivalent-layer model projected on a grid at a  
235 constant elevation by inverting full gravity-gradient data has the low-frequency error reduced by a factor of  
236 2.4 as compared to the inversion of an individual component of the gravity-gradient data.

## 237 2.2.5 The reparametrization of the equivalent layer

238 Oliveira Jr. et al. (2013) reparametrized the whole equivalent-layer model by a piecewise bivariate-  
239 polynomial function defined on a set of equivalent-source windows. By using a regularized potential-field  
240 inversion, Oliveira Jr. et al. (2013) estimates the polynomial coefficients for each equivalent-source window.  
241 After estimating all polynomial coefficients of all windows, the estimated coefficients are transformed  
242 into a single physical-property distribution encompassing the entire equivalent layer. This approach was

243 called "polynomial equivalent layer". As stated by Oliveira Jr. et al. (2013), the computational efficiency of  
 244 polynomial equivalent layer stems from the fact that the total number of polynomial coefficients required  
 245 to depict the physical-property distribution within the equivalent layer is generally much smaller than the  
 246 number of equivalent sources. Consequently, this leads to a considerably smaller linear system that needs  
 247 to be solved. Hence, the main strategy of polynomial equivalent layer is the model dimension reduction.

248 The polynomial equivalent layer was applied to perform upward continuations of gravity and magnetic  
 249 data and reduction to the pole of magnetic data.

## 250 2.2.6 The iterative scheme without solving a linear system

251 There exists a class of methods that iteratively estimate the distribution of physical properties within an  
 252 equivalent layer without the need to solve linear systems. The method initially introduced by Cordell (1992)  
 253 and later expanded upon by Guspí and Novara (2009) updates the physical property of sources, located  
 254 beneath each potential-field data, by removing the maximum residual between the observed and fitted data.  
 255 In addition, Xia and Sprowl (1991) and Xia et al. (1993) have developed efficient iterative algorithms for  
 256 updating the distribution of physical properties within the equivalent layer in the wavenumber and space  
 257 domains, respectively. Specifically, in Xia and Sprowl's (1991) method the physical-property distribution is  
 258 updated by using the ratio between the squared depth to the equivalent source and the gravitational constant  
 259 multiplied by the residual between the observed and predicted observation at the measurement station.  
 260 Neither of these methods solve linear systems.

261 Following this class of methods of iterative equivalent-layer technique that does not solve linear systems,  
 262 Siqueira et al. (2017) developed a fast iterative equivalent-layer technique for processing gravity data in  
 263 which the sensitivity matrix  $\mathbf{A}$  (equation 1) is replaced by a diagonal matrix  $N \times N$ , i.e.:

$$\tilde{\mathbf{A}} = 2\pi\gamma\Delta\mathbf{S}^{-1}, \quad (7)$$

264 where  $\gamma$  is Newton's gravitational constant and  $\Delta\mathbf{S}^{-1}$  is a diagonal matrix of order  $N$  whose diagonal  
 265 elements  $\Delta s_i$ ,  $i = 1, \dots, N$  are the element of area centered at the  $i$ th horizontal coordinates of the  $i$ th  
 266 observation point. The physical foundations of Siqueira et al.'s (2017) method rely on two constraints: i) the  
 267 excess of mass; and ii) the positive correlation between the gravity observations and the mass distribution  
 268 over the equivalent layer. By starting from a mass distribution on the equivalent layer, whose  $i$ th mass  $p_i^o$  is  
 269 proportional to the  $i$ th observed  $g_z$ -component data  $d_i^o$ ,

$$p_i^o = \frac{\Delta s_i d_i^o}{2\pi\gamma}, \quad (8)$$

270 Siqueira et al.'s (2017) method updates the mass distribution by adding mass corrections that are  
 271 proportional to the data residuals. At the  $k$ th iteration, the  $i$ th mass correction is given by:

$$\Delta\hat{p}_i^k = \frac{\Delta s_i r_i^k}{2\pi\gamma}, \quad (9)$$

272 where the  $i$ th data residual  $r_i^k$  is computed by subtracting the observed  $d_i^o$  from the fitted  $g_z$ -component  
 273 data  $d_i^k$  at the  $k$ th iteration, i.e.:

$$r_i^k = d_i^o - d_i^k. \quad (10)$$

274 Siqueira et al. (2017) applied their fast iterative equivalent-layer technique to interpolate, calculate the  
 275 horizontal components, and continue upward (or downward) gravity data.

276 For jointly process two gravity gradient components, Jirigalatu and Ebbing (2019) used the Gauss-FFT  
 277 for forward calculation of potential fields in the wavenumber domain combined with Landweber's iteration  
 278 coupled with a mask matrix  $M$  to reduce the edge effects without increasing the computation cost. The  
 279 mask matrix  $M$  is defined in the following way: if the corresponding pixel does not contain the original  
 280 data, the element of  $M$  is set to zero; otherwise, it is set to one. The  $k$ th Landweber iteration is given by

$$\mathbf{p}_{k+1} = \mathbf{p}_k + \omega \left[ \mathbf{A}_1^\top (\mathbf{d}_1 - M\mathbf{A}_1\mathbf{p}_k) + \mathbf{A}_2^\top (\mathbf{d}_2 - M\mathbf{A}_2\mathbf{p}_k) \right], \quad (11)$$

281 where  $\omega$  is a relaxation factor,  $\mathbf{d}_1$  and  $\mathbf{d}_2$  are the two gravity gradient components and  $\mathbf{A}_1$  and  $\mathbf{A}_2$  are the  
 282 corresponding gravity gradient kernels. Jirigalatu and Ebbing (2019) applied their method for processing  
 283 two horizontal curvature components of Falcon airborne gravity gradient.

#### 284 2.2.7 The convolutional equivalent layer with BTTB matrices

285 Takahashi et al. (2020, 2022) introduced the convolutional equivalent layer for gravimetric and magnetic  
 286 data processing, respectively.

287 Takahashi et al. (2020) demonstrated that the sensitivity matrix  $\mathbf{A}$  (equation 1) associated with a planar  
 288 equivalent layer formed by a set of point masses, each one directly beneath each observation point and  
 289 considering a regular grid of observation points at a constant height has a symmetric block-Toeplitz Toeplitz-  
 290 block (BTTB) structure. A symmetric BTTB matrix has, at least, two attractive properties. The first one is  
 291 that it can be defined by using only the elements forming its first column (or row). The second attractive  
 292 property is that any BTTB matrix can be embedded into a symmetric Block-Circulant Circulant-Block  
 293 (BCCB) matrix. This means that the full sensitivity matrix  $\mathbf{A}$  (equation 1) can be completely reconstruct  
 294 by using the first column of the BCCB matrix only. In what follows, Takahashi et al. (2020) computed  
 295 the forward modeling by using only a single equivalent source. Specifically, it is done by calculating the  
 296 eigenvalues of the BCCB matrix that can be efficiently computed by using only the first column of the  
 297 BCCB matrix via 2D fast Fourier transform (2D FFT). By comparing with the classic approach in the  
 298 Fourier domain, the convolutional equivalent layer for gravimetric data processing proposed by Takahashi  
 299 et al. (2020) performed upward- and downward-continue gravity data with a very small border effects and  
 300 noise amplification.

301 By using the original idea of the convolutional equivalent layer proposed by Takahashi et al. (2020)  
 302 for gravimetric data processing, Takahashi et al. (2022) proposed the convolutional equivalent layer for  
 303 magnetic data processing. By assuming a regularly spaced grid of magnetic data at a constant height and a  
 304 planar equivalent layer of dipoles, Takahashi et al. (2022) proved that the sensitivity matrix linked with  
 305 this layer possess a BTTB structure in the specific scenario where each dipole is exactly beneath each  
 306 observed magnetic data point. Takahashi et al. (2022) used a conjugate gradient algorithm (CGLS) which  
 307 does not require an inverse matrix or matrix-matrix multiplication. Rather, it only requires matrix-vector  
 308 multiplications per iteration, which can be effectively computed using the 2D FFT as a discrete convolution.  
 309 The matrix-vector product only uses the elements that constitute the first column of the associated BTTB  
 310 matrix, resulting in computational time and memory savings. Takahashi et al. (2022) showed the robustness  
 311 of the convolutional equivalent layer in processing magnetic survey that violates the requirement of regular  
 312 grids in the horizontal directions and flat observation surfaces. The convolutional equivalent layer was  
 313 applied to perform upward continuation of large magnetic datasets. Compared to the classical Fourier

314 approach, Takahashi et al.'s (2022) method produces smaller border effects without using any padding  
315 scheme.

316 Without taking advantage of the symmetric BTTB structure of the sensitivity matrix (Takahashi et al.,  
317 2020) that arises when gravimetric observations are measured on a horizontally regular grid, on a flat  
318 surface and considering a regular grid of equivalent sources whithin a horizontal layer, Mendonça (2020)  
319 explored the symmetry of the gravity kernel to reduce the number of forward model evaluations. By  
320 exploting the symmetries of the gravity kernels and redundancies in the forward model evaluations on a  
321 regular grid and combining the subspace solution based on eigenvectors of the gridded dataset, Mendonça  
322 (2020) estimated the mass excess or deficiency produced by anomalous sources with positive or negative  
323 density contrast.

### 3 NUMERICAL SIMULATIONS

324 We investigated different computational algorithms for inverting gravity disturbances and total-field  
 325 anomalies. To test the capability of the fast equivalent-layer technique for processing that potential field  
 326 data, we construct two tests. The first one is a measure of the computational effort by counting the number  
 327 of floating-point operations (*flops*), such as additions, subtractions, multiplications, and divisions (Golub  
 328 and Loan, 2013). For the results generated we are using  $it = 50$  for all the iterative methods.

329 **3.1 Floating-point operations calculation**

330 To measure the computational effort of the different algorithms to solve the equivalent layer linear system,  
 331 a non-hardware dependent method can be useful because allow us to do direct comparison between them.  
 332 Counting the floating-point operations (*flops*), i.e., additions, subtractions, multiplications and divisions is  
 333 a good way to quantify the amount of work of a given algorithm (Golub and Loan, 2013). For example,  
 334 the number of *flops* necessary to multiply two vectors  $\mathbb{R}^N$  is  $2N$ . A common matrix-vector multiplication  
 335 with dimension  $\mathbb{R}^{N \times N}$  and  $\mathbb{R}^N$ , respectively, is  $2N^2$  and a multiplication of two matrices  $\mathbb{R}^{N \times N}$  is  $2N^3$ .  
 336 Figure XX shows the total flops count for the different methods presented in this review with a crescent  
 337 number of data, ranging from 10,000 to 1,000,000.

338 **3.1.1 Normal equations using Cholesky decomposition**

339 The equivalent sources can be estimated directly from solving the normal equations 1. In this work we  
 340 will use the Cholesky decompositions method to calculate the necessary *flops*. In this method it is calculated  
 341 the lower triangule of  $\mathbf{A}^T \mathbf{A}$  ( $1/2N^3$ ), the Cholesky factor ( $1/3N^3$ ), a matrix-vector multiplication ( $2N^2$ )  
 342 and finally solving the triangular system ( $2N^2$ ), totalizing

$$f_{classical} = \frac{5}{6}N^3 + 4N^2 \quad (12)$$

343 **3.1.2 Window method (Leão and Silva, 1989)**

344 The moving data-window scheme (Leão and Silva, 1989) solve  $N$  linear systems with much smaller  
 345 sizes. For our results we are considering a data-window of the same size of which the authors presented  
 346 in theirs work ( $N_w = 49$ ) but, calculating with the same number of equivalent sources and not only the  
 347 one in the middle of the window. We are doing this process for all the other techniques to standardize the  
 348 resolution of our problem. Using the Cholesky decomposition with this method the *flops* are

$$f_{window} = N \frac{5}{6}N_w^3 + 4N_w^2 \quad (13)$$

349 **3.1.3 PEL method (Oliveira Jr. et al., 2013)**

350 The polynomial equivalent layer uses a similiar approach od moving windows from Leão and Silva  
 351 (1989). For this operations calculation we used a first degree polynomial (three variables) and each window  
 352 contains 1,000 observed data ( $N_s$ ). Following the steps given in (Oliveira Jr. et al., 2013) the total *flops*  
 353 becomes

$$f_{pel} = \frac{1}{3}H^3 + 2H^2 + 2NN_wH + H^2N + 2HN + 2NP \quad (14)$$

354 where  $H$  is the number of variable of the polynomial times the number of windows ( $3 \times N/1000$ ).

### 355 3.1.4 Conjugate gradient least square (CGLS)

356 The CGLS method is a very stable and fast algorithm for solving linear systems iteratively. Its computational complexity envolves a matrix-vector product outside the loop ( $2N^2$ ), two matrix-vector products inside the loop ( $4N^2$ ) and six vector products inside the loop ( $12N$ )

$$f_{ccls} = 2N^2 + it(4N^2 + 12N) \quad (15)$$

### 359 3.1.5 Wavelet compression method with CGLS (Li and Oldenburg, 2010)

360 For the wavelet method we have calculated a cocompression rate  $C_r$  of 98% of threshold as the authors in  
 361 Li and Oldenburg (2010) used and the wavelet transformation requiring  $\log_2(N)$  flops each, with its inverse  
 362 also using the same number of operations. Combined with the conjugate gradient least square necessary  
 363 steps and iterations, the number of flops are

$$f_{wavelet} = 2NC_r + 4N\log_2(N) + it(4N\log_2(N) + 4NC_r + 12C_r) \quad (16)$$

### 364 3.1.6 Fast equivalent layer for gravity data (Siqueira et al., 2017)

365 The fast equivalent layer from Siqueira et al. (2017) solves the linear system in  $it$  iterations. The main  
 366 cost of this method is the matrix-vector multiplication to asses the predicted data ( $2N^2$ ) and three simply  
 367 element by element vector sum, subtraction and division ( $3N$  total)

$$f_{siqueira} = it(3N + 2N^2) \quad (17)$$

### 368 3.1.7 Convolutional equivalent layer for gravity data (Takahashi et al., 2020)

369 This methods replaces the matrix-vector multiplication of the iterative fast-equivalent technique (Siqueira  
 370 et al., 2017) by three steps involving a Fourier transform and a inverse Fourier transform, and a Hadamard  
 371 product of matrices. Considering that the first column of our BCCB matrix has  $4N$  elements, the flops  
 372 count of this method is

$$f_{convgrav} = \kappa 4N \log_2(4N) + it(27N + \kappa 8N \log_2(4N)) \quad (18)$$

373 In the resultant count we considered a radix-2 algorithm for the fast Fourier transform and its inverse,  
 374 which has a  $\kappa$  equals to 5 and requires  $\kappa 4N \log_2(4N)$  flops each. The Hadarmard product of two matrices  
 375 of  $4N$  elements with complex numbers takes  $24N$  flops. Note that equation 18 is different from the one  
 376 presented in Takahashi et al. (2020) because we also added the flops necessary to calculate the eigenvalues  
 377 in this form. It does not differentiate much in order of magnitude because the iterative part is the most  
 378 costful.

## 379 3.1.8 Convolutional equivalent layer for magnetic data (Takahashi et al., 2022)

380 The convolutional equivalent layer for magnetic data uses the same flops count of the main operations as  
381 in the gravimetric case, the big difference is the use of the conjugate gradient algorithm to solve the inverse  
382 problem. It requires a Hadamard product outside of the iterative loop and more matrix-vector vector-vector  
383 multiplications inside the loop as seem in equation 15.

$$f_{convmag} = \kappa 16N \log_2(4N) + 24N + it(\kappa 16N \log_2(4N) + 60N) \quad (19)$$

## 384 3.1.9 Deconvolutional method

385 The deconvolution method does not require an iterative algorithm, rather it solves the estimative of the  
386 physical properties in a single step using the  $4N$  eigenvalues of the BCCB matrix as in the convolutional  
387 method. It requires a two fast Fourier transform ( $\kappa 4N \log_2(4N)$ ), one for the eigenvalues and another for  
388 the data transformation, a element by element division ( $24N$ ) and finally, a fast inverse Fourier transform  
389 for the final estimative ( $\kappa 4N \log_2(4N)$ ).

$$f_{deconv} = \kappa 12N \log_2(4N) + 24N \quad (20)$$

390 Using the deconvolutional method with a Wiener stabilization adds two multiplications of complex  
391 elements of the conjugates eigenvalues ( $24N$  each) and the sum of  $4N$  elements with the stabilization  
392 parameter  $\mu$

$$f_{deconvwiener} = \kappa 12N \log_2(4N) + 76N \quad (21)$$

## 4 SYNTHETIC DATA SIMULATIONS

393 For all applications, we generate a model composed by two spheres (PAREI AQUI - ANDRE)  
 394 Grav: the prism has a contrast of density equal to  $550\text{kg/m}^3$ , the left sphere  $600\text{kg/m}^3$  and the right sph-  
 395 ere  $-500\text{kg/m}^3$  All 3 bodies have magnetization of 3.46 intensity, 35.26 declination and 45.0 inclinations.  
 396 The grid of the synthetic data is 50x50.

397 **4.1 Stability analysis**

398 For the stability analysis we show the comparison of the normal equations solution with zeroth-order  
 399 Tikhonov regularization, the convolutional method for gravimetric and magnetic data, the deconvolutional  
 400 method and the deconvolutional method with different values for the Wiener stabilization. We create 21  
 401 data sets adding a crescent pseudo-random noise to the original data, which varies from 0% to 10% of  
 402 the maximum anomaly value, in intervals of 0.5%. These noises has mean equal to zero and a Gaussian  
 403 distribution. Figure XX shows how the residual between the predicted data and the noise-free data changes  
 404 as the level of the noise is increased. We can see that for all methods, a linear tendency can be observed as  
 405 it is expected. The inclination of the straight line is a indicative of the stability of each method. As show  
 406 in the graph the deconvolutional method is very unstable and it is really necessary to use a stabilization  
 407 method to have a good parameter estimative. In contrast, a correct value of the stabilization parameter is  
 408 necessary to not overshoot the smoothness of the solution as it is the case for the well-known zeroth-order  
 409 Tikhonov regularization. For the example using this gravimetric data, the optimal value for the Wiener  
 410 stabilization parameter is  $\mu = 10^{-9}$ . Figure XX shows the comparison of the predicted data for each  
 411 method with the original data.

412 For the magnetic data, the Wiener parameter seems to have the best solution for  $\mu = 10^{-13}$ . Figure XX  
 413 shows the comparison of the predicted data for each method with the original data.

414 Gravity synthetic statistics to be included:

415 Means

416 0.24791339230971493 (Classical method)

417 0.25522040542133817 (CG BTTB method)

418 0.86010282709889 (Deconvolutional method)

419 1.53835137193657 (Deconvolutional w Wiener overshoot  $\mu$  method)

420 0.3134732823974472 (Deconvolutional w Wiener optimal  $\mu$  method)

421 0.5553048046997608 (Deconvolutional w Wiener suboptimal  $\mu$  method)

422 Standard deviations

423 0.18274083156485463 (Classical method)

424 0.18986126212291252 (CG BTTB method)

425 1.439293452270024 (Deconvolutional method)

426 1.1183051446613188 (Deconvolutional w Wiener overshoot  $\mu$  method)

427 0.2367045031838225 (Deconvolutional w Wiener optimal  $\mu$  method)

428 0.7047326489645682 (Deconvolutional w Wiener suboptimal  $\mu$  method)  
429  
430 Magnetic synthetic statistics to be included:  
431 Means  
432 4.71700586977892 (Classical method)  
433 4.791561788289162 (CG BTTB method)  
434 2761.170136908849 (Deconvolutional method)  
435 23.06442216727077 (Deconvolutional w Wiener overshoot  $\mu$  method)  
436 8.860326967314595 (Deconvolutional w Wiener optimal  $\mu$  method)  
437 33.83142137645327 (Deconvolutional w Wiener suboptimal  $\mu$  method)  
438 Standard deviations  
439 3.571868619217408 (Classical method)  
440 3.6420538498453263 (CG BTTB method)  
441 4507.745135864884 (Deconvolutional method)  
442 14.232818621809827 (Deconvolutional w Wiener overshoot  $\mu$  method)  
443 7.445085208152109 (Deconvolutional w Wiener optimal  $\mu$  method)  
444 47.8175518946965 (Deconvolutional w Wiener suboptimal  $\mu$  method)

## 5 REAL DATA APPLICATION

445 Gridded data of 1000x500 (500000 observed points) for both grav and mag. Data is at -900m.  
446 Grav equivalent layer depth is 300 m and 50 iterations of the cgls method was used. Mag equivalent layer  
447 depth is 0 m and 200 iterations of the cgls method was used.  
448 On an Intel Core i7 7700HQ@2.8 GHz processor in single processing and single-threading modes the  
449 gravimetric equivalent layer took 9.19 seconds to estimate the equivalent sources with the convolutional  
450 method and 0.51 seconds with the deconvolutional method.  
451 The magnetic equivalent layer took 82 seconds to estimate the equivalent sources with the convolutional  
452 method and 0.84 seconds with the deconvolutional method.  
453 As Carajás area is very large different values of the magnetic main field can be considered.  
454 The main field declination was calculated using the tool in the website (for the date 01/01/2014):  
455 <https://www.ngdc.noaa.gov/geomag/calculators/magcalc.shtml> For this application I considered an approximated mid location of the area (latitude  $-6.55^\circ$  and longitude  $-50.75^\circ$ ). The declination is  $-19.865^\circ$   
456 and the inclination  $-7.43915^\circ$ . As the source magnetization is unknown inclination and declination equal  
457 to the main field is being used for all the equivalent sources.  
458

459 Gravimetric case:  
460 Means  
461 0.0005096975472675431 (convolutional method)  
462 0.4582999511463665 (deconvolutional method with wiener  $\mu = 10^{-22}$ )  
463 Standart deviations  
464 0.15492798729938298 (convolutional method)  
465 1.229507199000529 (deconvolutional method with wiener  $\mu = 10^{-22}$ )  
466  
467 Magnetic case:  
468 Means  
469 -0.06404347121632468 (convolutional method)  
470 18.992921718679344 (deconvolutional method with wiener  $\mu = 10^{-16}$ )  
471 Standart deviations  
472 1.9687559764381535 (convolutional method)  
473 33.641199020925924 (deconvolutional method with wiener  $\mu = 10^{-16}$ )

## 6 DISCUSSION AND CONCLUSION

## CONFLICT OF INTEREST STATEMENT

474 The authors declare that the research was conducted in the absence of any commercial or financial  
475 relationships that could be construed as a potential conflict of interest.

## AUTHOR CONTRIBUTIONS

476 The Author Contributions section is mandatory for all articles, including articles by sole authors. If an  
477 appropriate statement is not provided on submission, a standard one will be inserted during the production  
478 process. The Author Contributions statement must describe the contributions of individual authors referred  
479 to by their initials and, in doing so, all authors agree to be accountable for the content of the work. Please  
480 see here for full authorship criteria.

## FUNDING

481 Diego Takahashi was supported by a Post-doctoral scholarship from CNPq (grant 300809/2022-0) Valéria  
482 C.F. Barbosa was supported by fellowships from CNPq (grant 309624/2021-5) and FAPERJ (grant  
483 26/202.582/2019). Vanderlei C. Oliveira Jr. was supported by fellowships from CNPq (grant 315768/2020-  
484 7) and FAPERJ (grant E-26/202.729/2018).

## ACKNOWLEDGMENTS

485 We thank the Brazilian federal agencies CAPES, CNPq, state agency FAPERJ and Observatório Nacional  
486 research institute and Universidade do Estado do Rio de Janeiro.

## DATA AVAILABILITY STATEMENT

487 The datasets generated for this study can be found in the frontiers-paper Github repository link:  
488 <https://github.com/DiegoTaka/frontiers-paper>.

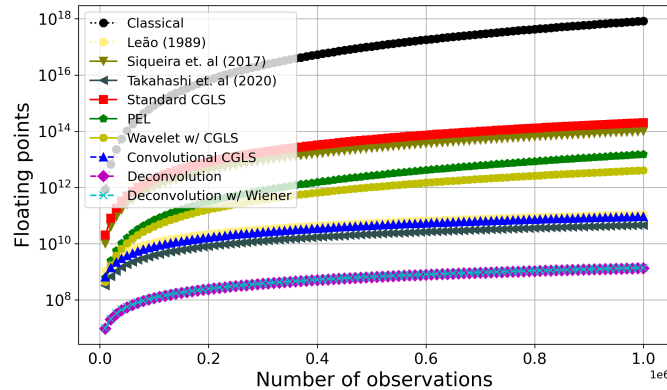
## REFERENCES

- 489 Aster, R. C., Borchers, B., and Thurber, C. H. (2018). *Parameter estimation and inverse problems*  
490 (Elsevier)
- 491 Barbosa, V. C. F., Silva, J. B., and Medeiros, W. E. (1997). Gravity inversion of basement relief using  
492 approximate equality constraints on depths. *Geophysics* 62, 1745–1757
- 493 Barnes, G. and Lumley, J. (2011). Processing gravity gradient data. *Geophysics* 76, I33–I47. doi:10.1190/  
494 1.3548548
- 495 Cordell, L. (1992). A scattered equivalent-source method for interpolation and gridding of potential-field  
496 data in three dimensions. *Geophysics* 57, 629–636
- 497 Dampney, C. N. G. (1969). The equivalent source technique. *Geophysics* 34, 39–53. doi:10.1190/1.  
498 1439996
- 499 Davis, K. and Li, Y. (2011). Fast solution of geophysical inversion using adaptive mesh, space-filling  
500 curves and wavelet compression. *Geophysical Journal International* 185, 157–166. doi:10.1111/j.  
501 1365-246X.2011.04929.x
- 502 Friedman, J. H. (2001). Greedy function approximation: a gradient boosting machine. *Annals of statistics* ,  
503 1189–1232

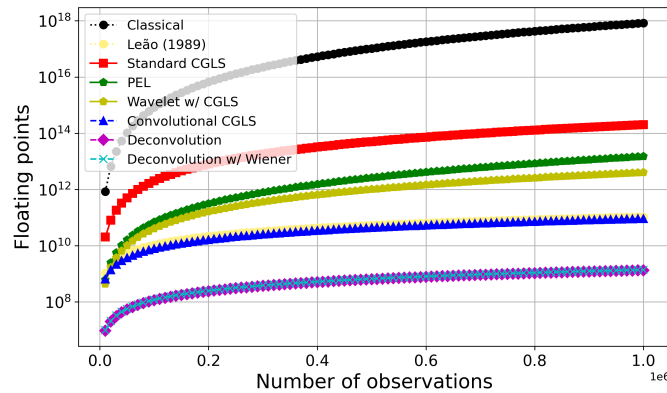
- 504 Friedman, J. H. (2002). Stochastic gradient boosting. *Computational statistics and data analysis* 38,  
505 367–378
- 506 Golub, G. H. and Loan, C. F. V. (2013). *Matrix Computations (Johns Hopkins Studies in the Mathematical  
507 Sciences)* (Johns Hopkins University Press), 4 edn.
- 508 Guspí, F. and Novara, I. (2009). Reduction to the pole and transformations of scattered magnetic data using  
509 newtonian equivalent sources. *Geophysics* 74, L67–L73
- 510 Jirigalatu, J. and Ebbing (2019). A fast equivalent source method for airborne gravity gradient data.  
511 *Geophysics* 84, G75–G82. doi:10.1190/GEO2018-0366.1
- 512 Kellogg, O. D. (1929). *Foundations of Potential Theory* (Frederick Ungar Publishing Company)
- 513 Kennett, B., Sambridge, M., and Williamson, P. (1988). Subspace methods for large inverse problems with  
514 multiple parameter classes. *Geophysical Journal International* 94, 237–247
- 515 Leão, J. W. D. and Silva, J. B. C. (1989). Discrete linear transformations of potential field data. *Geophysics*  
516 54, 497–507. doi:10.1190/1.1442676
- 517 Li, Y. and Oldenburg, D. W. (2010). Rapid construction of equivalent sources using wavelets. *Geophysics*  
518 75, L51–L59. doi:10.1190/1.3378764
- 519 Mendonça, C. A. (2020). Subspace method for solving large-scale equivalent layer and density mapping  
520 problems. *Geophysics* 85, G57–G68. doi:10.1190/geo2019-0302.1
- 521 Mendonça, C. A. and Silva, J. B. C. (1994). The equivalent data concept applied to the interpolation of  
522 potential field data. *Geophysics* 59, 722–732. doi:10.1190/1.1443630
- 523 Oldenburg, D., McGillivray, P., and Ellis, R. (1993). Generalized subspace methods for large-scale inverse  
524 problems. *Geophysical Journal International* 114, 12–20
- 525 Oliveira Jr., V. C., Barbosa, V. C. F., and Uieda, L. (2013). Polynomial equivalent layer. *Geophysics* 78,  
526 G1–G13. doi:10.1190/geo2012-0196.1
- 527 Siqueira, F. C., Oliveira Jr, V. C., and Barbosa, V. C. (2017). Fast iterative equivalent-layer technique for  
528 gravity data processing: A method grounded on excess mass constraint. *Geophysics* 82, G57–G69
- 529 Skilling, J. and Bryan, R. (1984). Maximum entropy image reconstruction-general algorithm. *Monthly  
530 Notices of the Royal Astronomical Society, Vol. 211, NO. 1, P. 111, 1984* 211, 111
- 531 Soler, S. R. and Uieda, L. (2021). Gradient-boosted equivalent sources. *Geophysical Journal International*  
532 227, 1768–1783. doi:10.1093/gji/ggab297
- 533 Takahashi, D., Oliveira, V. C., and Barbosa, V. C. (2022). Convolutional equivalent layer for magnetic data  
534 processing. *Geophysics* 87, 1–59
- 535 Takahashi, D., Oliveira Jr, V. C., and Barbosa, V. C. (2020). Convolutional equivalent layer for gravity data  
536 processing. *Geophysics* 85, G129–G141
- 537 Xia, J. and Sprowl, D. R. (1991). Correction of topographic distortion in gravity data. *Geophysics* 56,  
538 537–541
- 539 Xia, J., Sprowl, D. R., and Adkins-Helgeson, D. (1993). Correction of topographic distortions in potential-  
540 field data; a fast and accurate approach. *Geophysics* 58, 515–523. doi:10.1190/1.1443434

## 7 SUPPLEMENTARY TABLES AND FIGURES

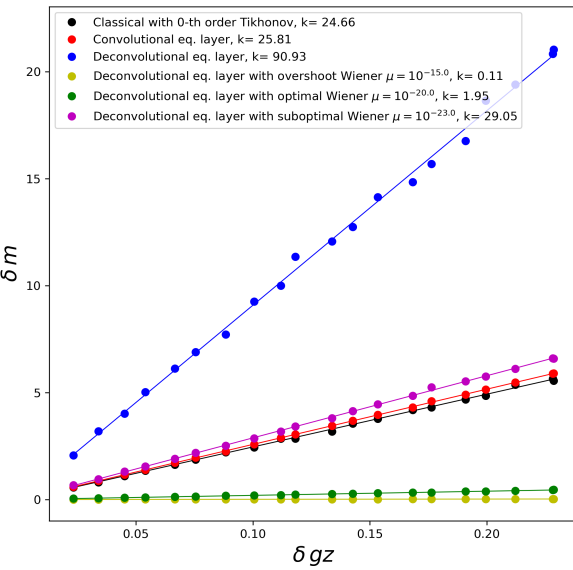
### 541 7.1 Figures



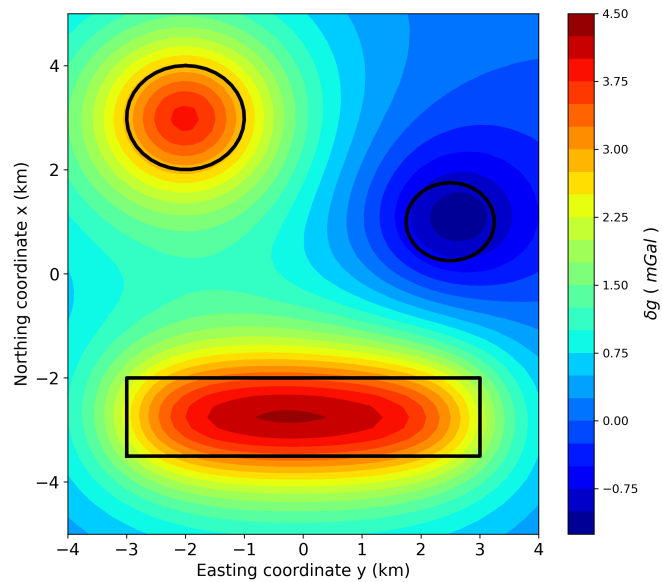
**Figure 1.** Number of *flops* for some of the methods to estimate the equivalent sources of the gravimetric case.



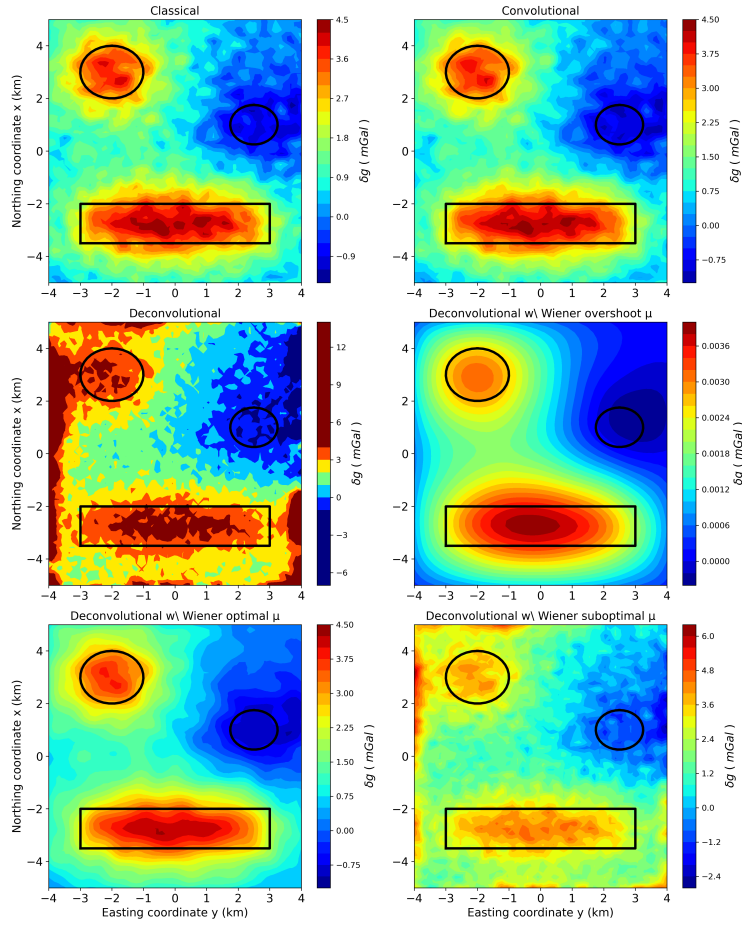
**Figure 2.** Number of *flops* for some of the methods to estimate the equivalent sources of the magnetic case.



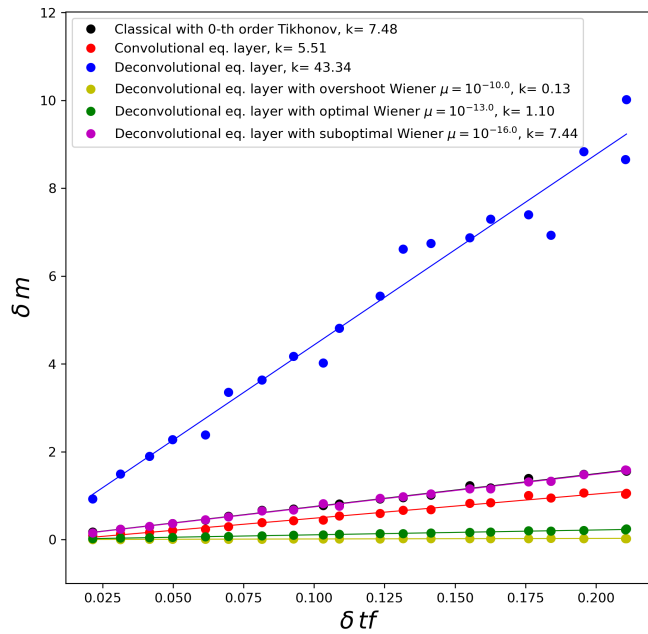
**Figure 3.** Stability analysis of some of the equivalent layer methods of the gravimetric case.



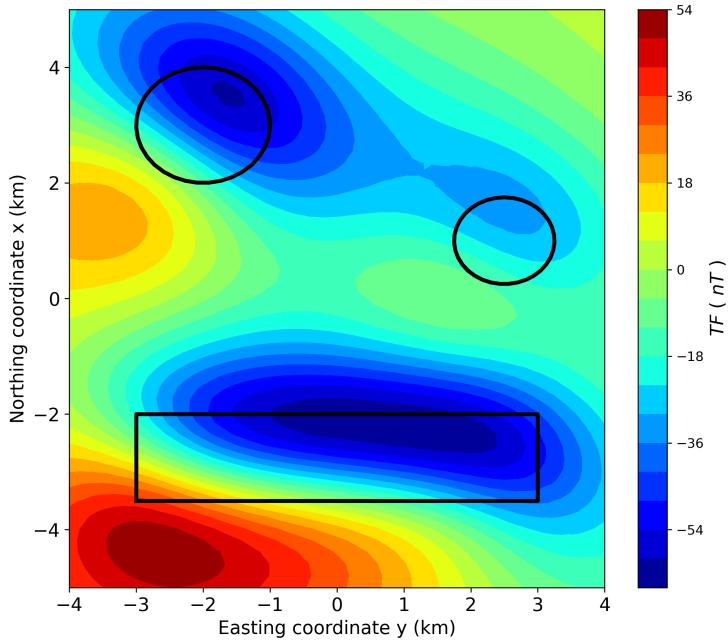
**Figure 4.** Synthetic noise-free data of the gravimetric case.



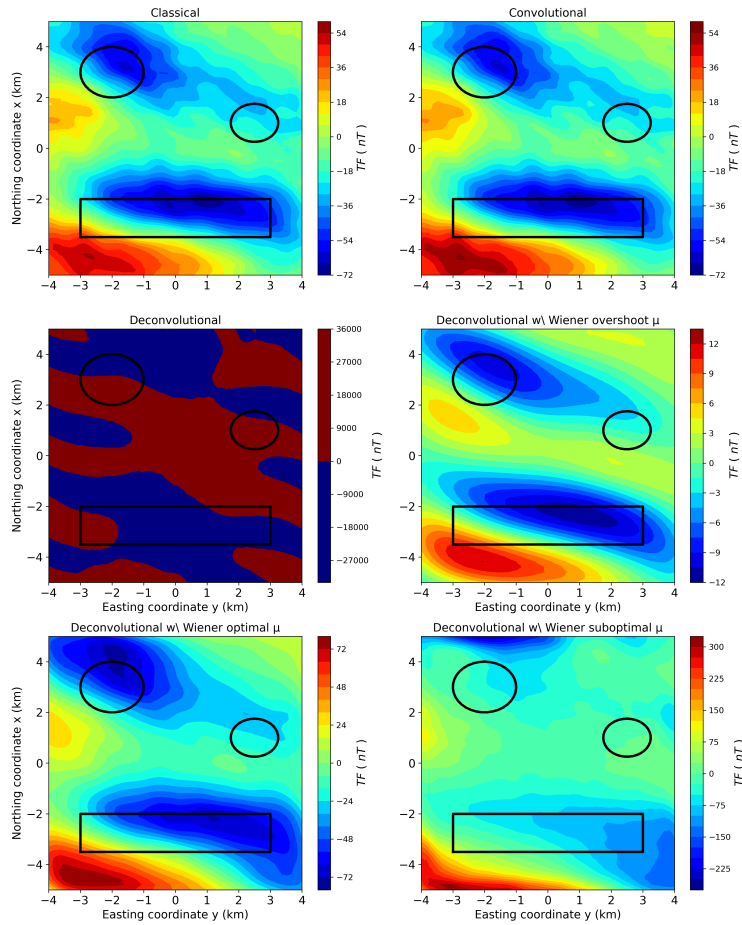
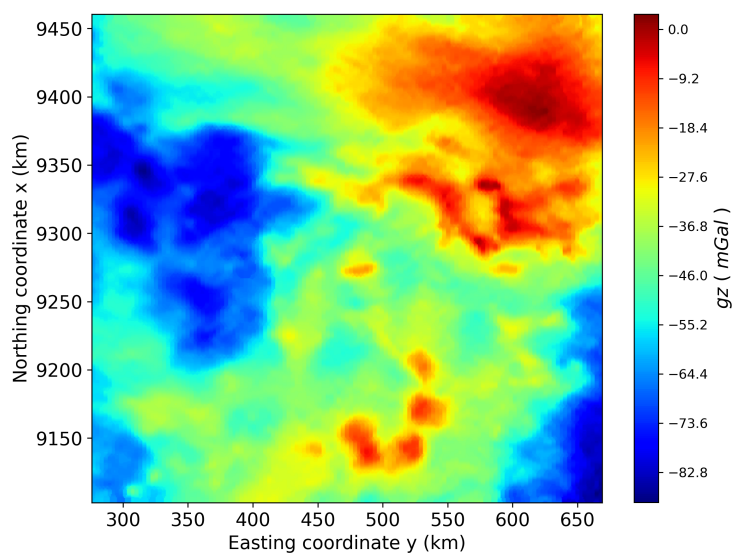
**Figure 5.** Predicted gravity data for different methods of the equivalent layer with maximum level of noise. Panel (A) is the classical method, (B) is the convolutional, (C) is the deconvolutional, (D) is the deconvolutional method using Wiener stabilization with a too high value for  $\mu$ , (E) is the deconvolutional method using Wiener stabilization with an optimal value for  $\mu$  and (F) is the deconvolutional method using Wiener stabilization with a too low value for  $\mu$ .



**Figure 6.** Stability analysis of some of the equivalent layer methods of the magnetic case.



**Figure 7.** Synthetic noise-free data of the magnetic case.

**Figure 8.****Figure 9.** Gridded real aerogravimetric data from Carajás, Brazil.

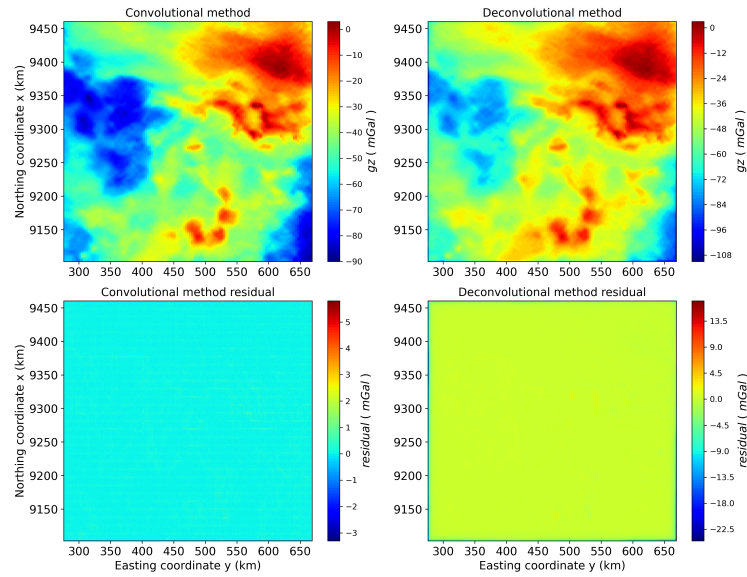


**Figure 10.** Panel (A) shows the predicted data from convolutional equivalent layer method. Panel (B) shows the residual from the convolutional equivalent layer method. Panel (C) shows the predicted data from deconvolutional equivalent layer method. Panel (D) shows the residual from the deconvolutional equivalent layer method.

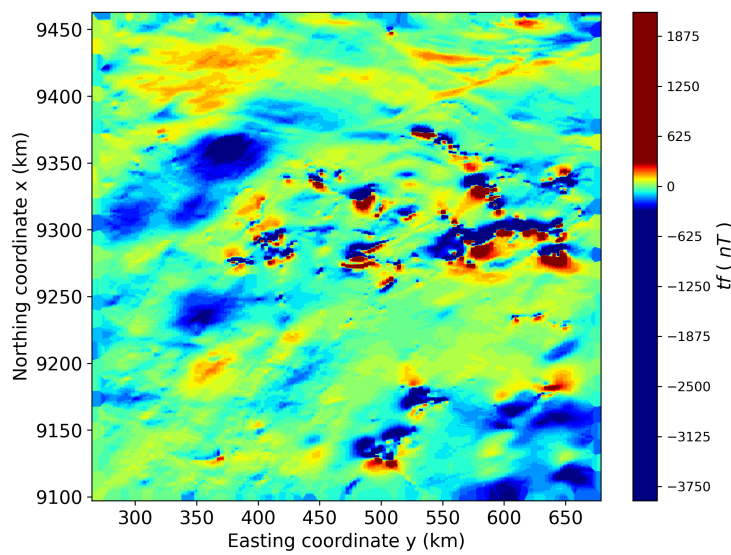


**Figure 11.** Gridded real aeromagnetic data from Carajás, Brazil.

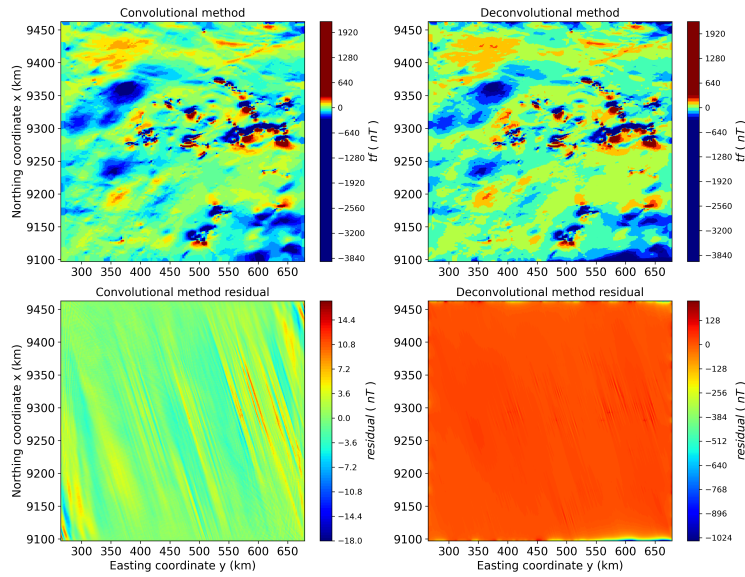


**Figure 12.** Panel (A) shows the predicted data from convolutional equivalent layer method. Panel (B) shows the residual from the convolutional equivalent layer method. Panel (C) shows the predicted data from deconvolutional equivalent layer method. Panel (D) shows the residual from the deconvolutional equivalent layer method.